Journal of the Civil Engineering Forum, May 2024, 10(2):109-122
DOI 10.22146/jcef.9713
Available Online at https://jurnal.ugm.ac.id/v3/jcef/issue/archive

Excess Pore Pressure Migration Analysis Due to High Embankment Construction – Case Study East Kalimantan

Edwin Lie, Paulus Pramono Rahardjo, Martin Wijaya*
Department of Civil Engineering, Faculty of Engineering, Parahyangan Catholic University, Bandung, INDONESIA
Jalan Ciumbeluit No.94
*Corresponding author: mwijaya@unpar.ac.id

SUBMITTED 19 September 2023 **REVISED** 11 January 2024 **ACCEPTED** 19 January 2024

ABSTRACT A 42-inch pipeline traverses a predominantly flat right-of-way (ROW), running from south to north in East Kalimantan. Adjacent to the ROW, a coal mine concession was located on the western side, while the Mahakam River lies a further 3 km to the east. A mining waste dump has been constructed since 2010, situated in an area underlain by soft alluvium soil (Q_a). The waste was stacked, reaching heights of up to 75 meters, with its toe approximately 200 m from the edge of the ROW. In 2016, a failure occurred in the ROW, causing the 42-inch pipeline to shift a maximum of 6.8 m horizontally, and rise by 2.0 m within a 300 m span. A geotechnical investigation was then conducted, consisting of 7 CPTu with dissipation testing. The CPTu results indicated high pore pressure, with a layer of soft clay ranging from 15 to 32 m thickness found in the ROW area. A hypothesis was formulated suggesting that the soft clay was not fully consolidated. Hence, the failure of the pipeline was possibly caused by the migration of excess pore water pressure accumulated during the construction of the waste dump. Results of the investigation indicated that the permeability coefficient was 2.5 times greater in the horizontal direction compared to the vertical ones (k_h/k_v = 2.5), allowing the pore water pressure to migrate more easily in the horizontal direction. This study aims to elucidate how the migration of excess pore water pressure in the horizontal direction influences ground stability. The analysis was conducted using finite element software MIDAS GTS NX, with the k_h/k_v varying from 2.5 to 100 times to explore excess pore pressure movement behaviors. The results of this study confirm that excess pore pressure migration can occur horizontally if the horizontal permeability coefficient is larger than its vertical counterpart. Thus, this study highlights that the greater the permeability coefficient and the larger the ratio, the further the excess pore pressure travels. Moreover, the horizontal displacement increases with the permeability coefficient ratio.

KEYWORDS Alluvium; Soft Clay; Consolidating; Excess Pore Pressure; Migration; Permeability

1 INTRODUCTION

Failure in an oil and gas pipeline can occur due to either the effects of external forces or the degradation of its internal integrity. External forces can cause dents, cracks, or bends, which ultimately compromise the mechanical properties of the pipeline (Visnuvardhan et al., 2023). Landslides or ground failures are one of the most critical external forces affecting the pipeline. Numerous studies have investigated the behavior of buried pipelines subjected to axial and lateral forces due to ground failure (e.g., (Trautmann and O'Rourke, 1985; Shen et al., 2009; Yuan et al., 2014; Al-Khazaali and Vanapalli, 2018; Zhang and Askarinejad, 2021). Nevertheless, most of these studies were based on laboratory tests involving sand material and rainfall influence, yet none involving soft clay and excess pore pressure.

A 50 m wide pipeline right-of-way (ROW) ran south-to-north in East Kalimantan. The ROW area was relatively flat, located approximately 3 km east of the Mahakam River and adjacent to a coal mine concession on the west side. An overburden waste dump has been constructed approximately 2 kilometers west of the ROW since 2010. The toe of the dump is approximately 200 m away from the edge of the ROW. An overhead conveyor was fully constructed in 2015, extending across the ROW from west to east. Shortly after the completion of the conveyor, a failure occurred in its foundation, causing it to tilt. The conveyor then collapsed and was subsequently dismantled. In 2016, the ground heaved and bulged, extending 300 m in length, and appeared in the west part of the ROW. Topographic surveys indicated that the 42-inch pipeline was affected, experiencing shifting and bending with a maximum deflection of 6.8 m horizontally and 2.0 m vertically. This study aims to delineate the failure mechanism resulting from the overburden waste dump, which led to the deflection in the pipeline. The failure mechanism of the waste dump was attributed to the migration of excess pore pressure during the construction phase.

2 GEOLOGICAL GEOTECHNICAL CONDITION

According to the 1995 geological map of Samarinda City, issued by the Geological Research Development Center of Indonesia, the site was located between Ba-

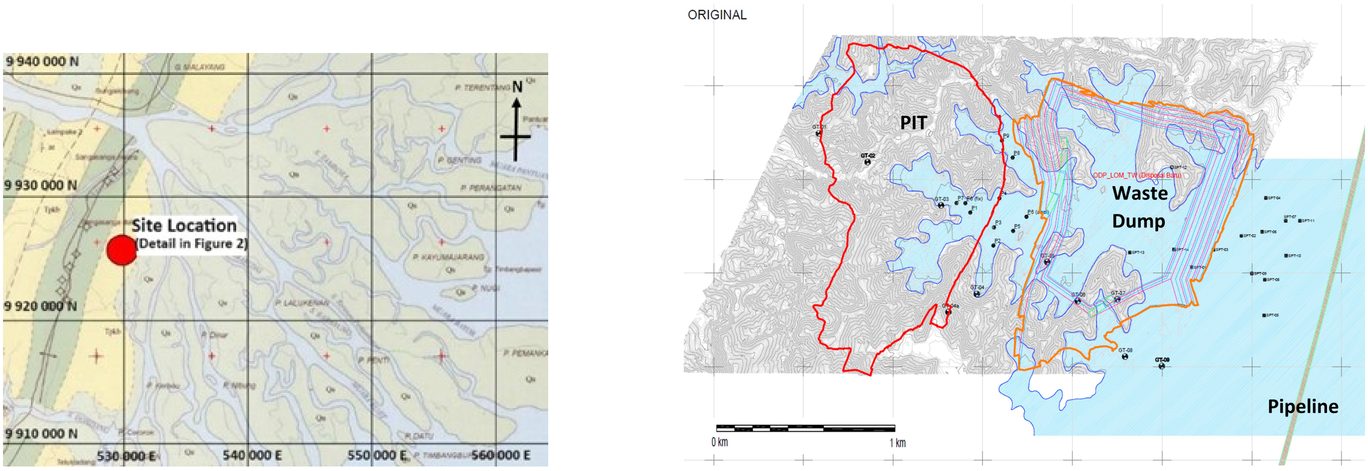

(a) (b)

Figure 1 Geological map (a) and detailed geological map (b)

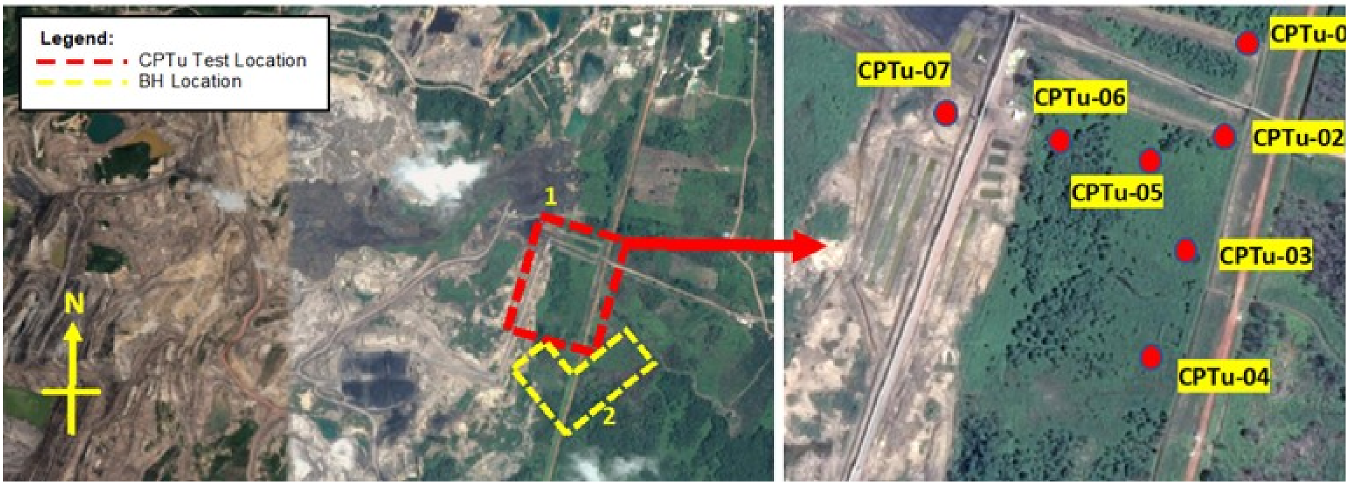

Figure 2 Area layout (left) and geotechnical investigation layout (right)

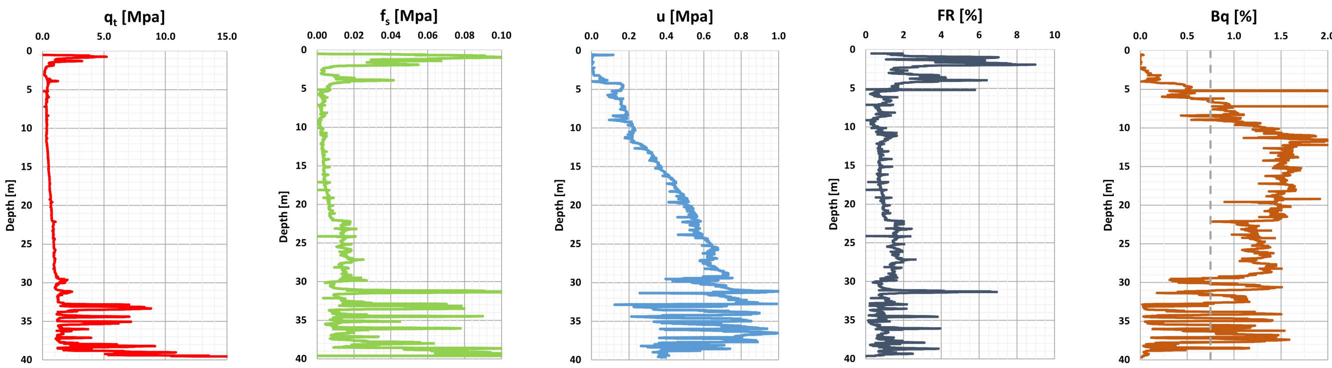

(a) (b) (c) (d) (e)

Figure 3 Test result from CPTu-02: corr. cone resistance (a), sleeve friction (b), pore pressure (c), friction ratio (d), pore pressure ratio (e)

likpapan Formation (Tmbp) and Kampung Baru Formation (Tpkb). An alluvium formation (Qa) was located on the east side of the site. The detailed geological map presented in Figure 1 indicated the presence of soft clay alluvium beneath the overburden waste dump.

Geotechnical investigations, consisting of 7 CPTu and 12 dissipation tests, were conducted between August and September 2016. These tests were performed in the area between the toe of the dump and the edge of the ROW, as depicted in Figure 2, within the red dashed

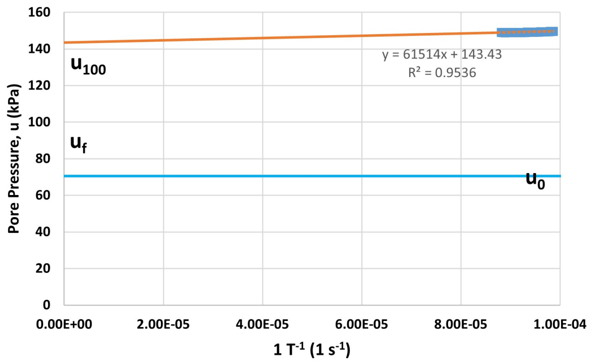

(a)

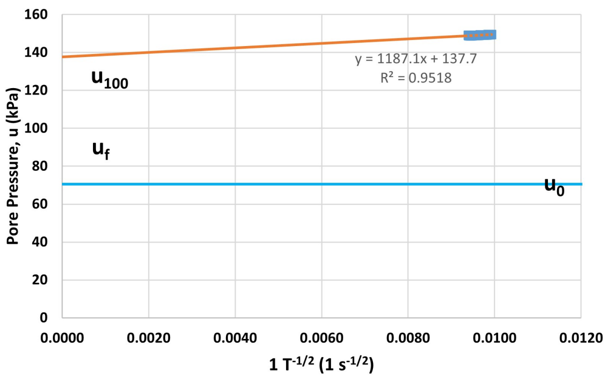

(b)

Figure 4 CPTu-02 dissipation test interpretation at depth 9.18 m using inverse time method (a) and inverse square root time method (b)

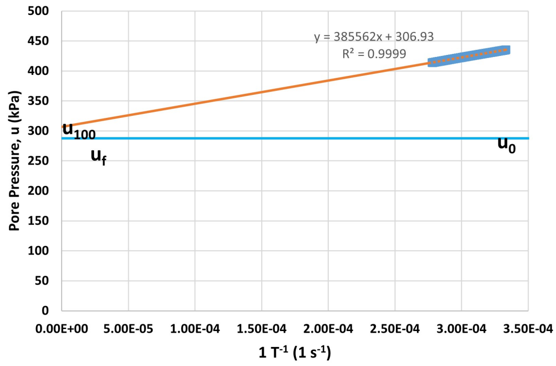

(a)

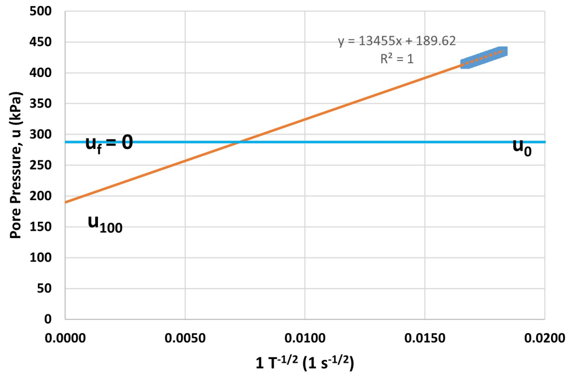

(b)

Figure 5 CPTu-02 dissipation test interpretation at depth 31.34 m using inverse time method (a) and inverse square root time method (b)

Table 1. Dissipation test details

CPTu ID	Elevation	GWL	Dissipation				
			Depth	Duration	B_q	u_i	u_0
	[m]	[m]	[m]	[s]	[%]	[kPa]	[kPa]
CPTu-01	6.65	0.0	3.91	3799	0.44	139.70	31.78
			12.50	362	1.78	301.30	122.63
			27.92	2908	1.31	743.50	267.32
CPTu-02	6.62	2.0	9.18	11340	1.00	208.00	70.44
			31.34	3600	0.57	883.70	287.83
CPTu-03	6.24	4.0	4.11	10500	0.17	95.583	1.08
			6.76	3327	0.42	165.32	27.08
			9.90	8580	0.68	250.17	57.88
CPTu-04	4.55	1.0	12.63	8460	0.89	378.87	114.09
CPTu-05	8.13	1.5	15.11	10080	1.25	330.20	133.51
CPTu-06	11.09	4.0	18.72	9210	2.48	361.10	144.40
CPTu-07	12.32	2.0	22.27	9210	1.08	529.10	198.05
CPTu-08A	12.86	2.0	21.55	8130	1.30	531.82	191.78
CPTu-09A	8.47	0.0	15.2	14850	1.60	337.64	149.11
CPTu-09B	7.79	2.40	3.51	2160	0.31	137.0	55.0
			8.86	4350	0.27	236.0	162.0
CPTu-10A	5.64	0.0	9.73	11130	0.90	215.19	95.45
			30.59	2340	1.00	692.39	300.09

rectangle. Results of the tests indicated the existence of a 15 to 32 m thick layer of soft soil beneath the area, followed by stiff to hard clays and dense to very dense sands. Further assessment of the dissipation test results revealed that, although the duration of the test was estimated based on the initial pore water pressure and hydrostatic pressure, most tests terminated before reaching u_{50}. The typical result of the CPTu test is presented in Figure 3, while the details of the dissipation test are provided in Table 1.

Numerous methods have been developed to correct and interpret the dissipation test results (Sully et al., 1999; Whittle et al., 2001; Balachowski, 2006; Chai et al., 2012; Chung et al., 2014; Zhang et al., 2022). In this paper, we employed the inverse time method (Lim et al., 2014) and the inverse square root time method (Liu et al., 2014) to interpret the incomplete dissipation data. The interpretation involves interpolating the end part of the dissipation test curve plotted with time or the square root time. The point of intersection with the pore pressure indicates the residual pore pressure. The residual pore pressure was then compared with the hydrostatic pore pressure. If the residual pore pressure exceeds the hydrostatic pore pressure, the soil is still undergoing consolidation. The interpretation of all dissipation tests conducted at the location suggested that the soft clay is still undergoing consolidation. A typical dissipation interpretation using the inverse time method and the inverse square root method is presented in Figure 4 and Figure 5 and summarized in Table 2.

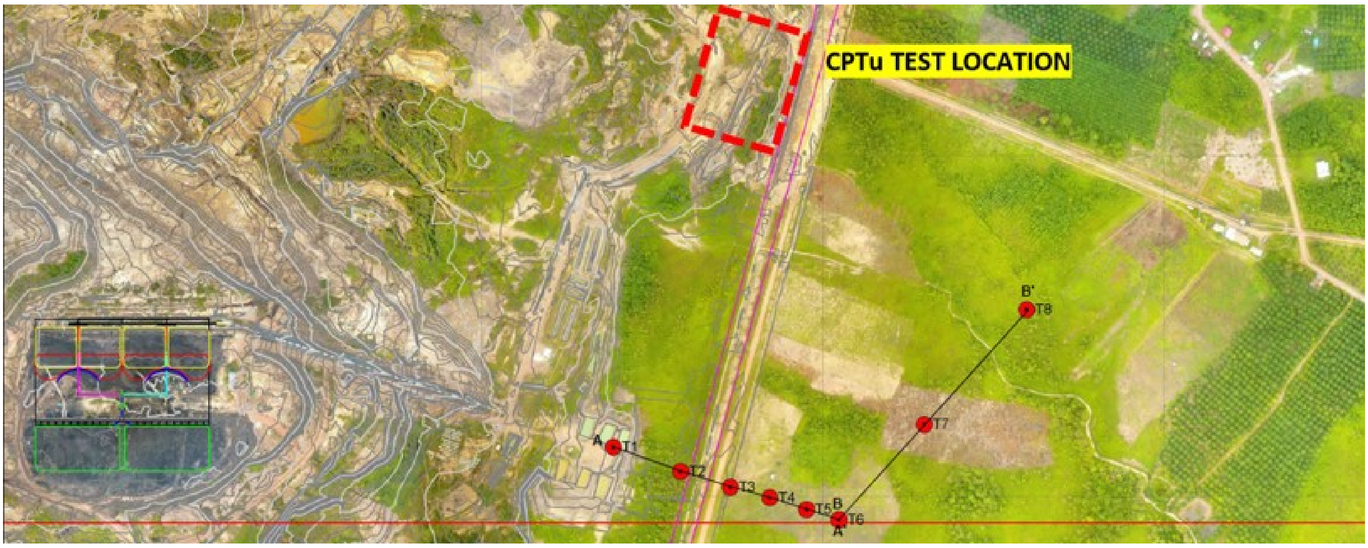

Figure 6 Borehole test location

Table 2. Dissipation interpretation

CPTu	Test Information			Inverse Time Method		Inverse Square Root Time Method		
ID	Depth [m]	GWL [m]	u_0 [kPa]	u_{100} [kPa]	u_f [kPa]	u_{100} [kPa]	u_f [kPa]	Remarks
CPTu-01	3.91	0.0	31.78	20.03	0	0.00	0	No excess PWP
	12.50		122.63	264.03	141.40	252.31	129.69	Still Consolidating
	27.92		267.32	429.10	161.78	337.41	70.09	Still Consolidating
CPTu-02	9.18	2.0	70.44	143.43	72.99	137.70	67.26	Still Consolidating
	31.34		287.83	306.93	19.10	189.62	0	No excess PWP
CPTu-03	4.11	4.0	1.08	69.12	68.04	61.97	60.89	No excess PWP
	6.76		27.08	78.49	51.41	65.39	38.31	Still Consolidating
	9.90		57.88	123.70	65.82	106.28	48.40	Still Consolidating
CPTu-04	12.63	1.0	114.09	159.96	45.87	113.19	0	Both Method Contradicts
CPTu-05	15.11	1.5	133.51	246.20	112.69	230.90	97.39	Still Consolidating
CPTu-06	18.72	4.0	144.40	324.52	180.12	319.93	175.53	Still Consolidating
CPTu-07	22.27	2.0	198.05	348.23	149.38	313.76	114.91	Still Consolidating

Note: PWP = Pore Water Pressure

Further to the south, approximately 500 m from the CPTu test location, a geotechnical investigation comprising eight boreholes was carried out between March and May 2018 to construct a new overhead conveyor. The boreholes (BH) locations are indicated by the yellow dashed rectangle in Figure 2. This investigation includes performing Standard Penetration Test (SPT), undisturbed (UD) sampling, and laboratory testing. The layout of the BH tests is shown in Figure 6. Borehole T1 was excluded due to its location in a hill-cut area, while boreholes T2 and T3 were discarded due to their proximity to the pipeline inspection road. The typical description of BH is presented in Table 3.

3 SOIL PARAMETERS

The soil layering was classified into two distinct layers: soft and hard clay. Soil parameters were determined from both dissipation and laboratory test results. Laboratory tests included index properties, Atterberg limits, grain-size analysis, triaxial UU, direct shear, and consolidation tests. The results of laboratory tests, along with the adopted values, are presented in Figures 7, 8, 9 and 10. The consolidation coefficient was estimated following the method proposed by Teh and Houlsby (1991), while the permeability coefficient was determined using the correlation provided by Robertson (2010). The results of these analyses are summarized in Table 4. The parameters used for the analysis are summarized in Table 5.

3.1 Result

The effective friction angle of the soil was derived using the relationship from the Plasticity Index (PI) developed by Terzaghi et al. (1996), as shown in Figure

Table 3. Borehole SPT and soil description

BH-T4				BH-T5				BH-T8			
Depth [m]	Soil Type	N-SPT	Plot	Depth [m]	Soil Type	N-SPT	Plot	Depth [m]	Soil Type	N-SPT	Plot
2.00	Silty CLAY	0		1.00	Silty CLAY	1		2.00	Silty CLAY	0	
4.00	Silty SAND	0		3.00	Silty SAND	0		5.00	Silty CLAY	0	
6.00	Silty SAND	13		5.00	Silty SAND	0		7.00	Silty CLAY	0	
8.00	Silty SAND	11		7.00	Silty SAND	10		9.00	Silty CLAY	0	
10.00	Silty SAND	0		9.00	Silty SAND	1		12.00	Silty CLAY	0	
12.00	Silty CLAY	0		11.00	Silty CLAY	0		14.00	Silty CLAY	0	
14.00	Silty CLAY	3		13.00	Silty CLAY	0		17.00	Silty CLAY	0	
16.00	Silty CLAY	0		15.00	Silty CLAY	0		19.00	Silty CLAY	0	
19.00	Silty CLAY	0		17.00	Silty CLAY	0		21.00	Silty CLAY	0	
21.00	Silty CLAY	3		19.00	Silty CLAY	0		23.00	Silty CLAY	0	
24.00	Silty CLAY	2		20.00	Silty CLAY	0		25.75	Silty CLAY	11	
26.00	Silty CLAY	9		22.00	Silty CLAY	1		28.00	Silty CLAY	6	
28.00	Silty CLAY	23		25.00	Silty CLAY	5		30.75	Silty SAND	7	
30.00	Silty CLAY	33		27.00	Silty CLAY	7		33.00	Silty CLAY	8	
32.00	Silty CLAY	44		29.00	Silty CLAY	41		35.75	Silty SAND	21	
34.00	Silty CLAY	42		31.00	Silty CLAY	25		38.00	Silty SAND	50	
36.00	Silty CLAY	50		33.00	Silty CLAY	45		40.00	Silty SAND	30	
38.00	Silty CLAY	50		35.00	Silty CLAY	50		42.00	Silty SAND	50	
40.00	Silty CLAY	50		37.00	Silty SAND	50		44.00	Silty SAND	50	
42.00	Silty CLAY	50		39.00	Silty SAND	50		46.00	Silty SAND	50	
44.00	Silty CLAY	50		41.00	Silty SAND	50		48.00	Silty SAND	50	
46.00	Silty CLAY	50		43.00	Silty SAND	50					
48.00	Silty SAND	50		45.00	Silty SAND	50					
				47.00	Silty SAND	50					

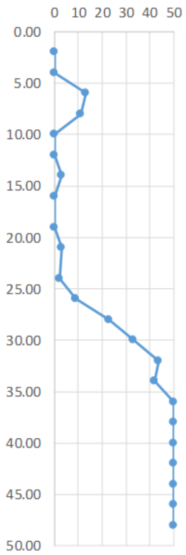

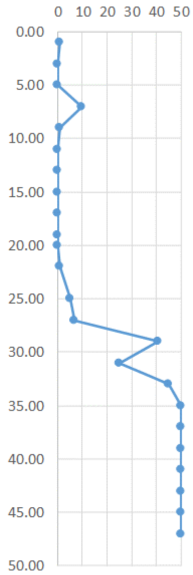

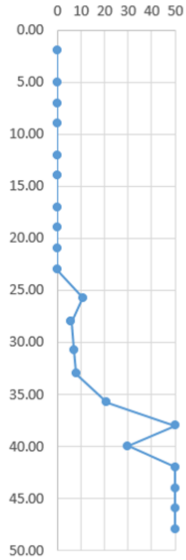

Table 4. Coefficient of permeability parameters

Parameter	Symbol	Unit	Soft Clay	Hard Clay
Horizontal Coefficient of Consolidation	c_h	cm^2s^{-1}	0.0025	0.0010
		m^2s^{-1}	2.50E-07	1.00E-07
Vertical Coefficient of Consolidation	c_v	cm^2s^{-1}	0.0010	0.0010
		m^2s^{-1}	1.00E-07	1.00E-07
Normalized Cone Resistance	Q_{tn}		2.00	5.00
Normalized Friction Ratio	F_r		2.00	1.00
Soil Behavior Type Index	I_c		11.56	8.90
Parameter related Modulus	α_M		2	5
Net Cone Resistance	q_n	kN m^{-2}	400	800
1-D Constraint Modulus	M		800	4000
Horizontal Permeability Coefficient	k_h	m s^{-1}	3.07E-09	2.45E-10
		m day^{-1}	2.65E-04	2.12E-05
Vertical Permeability Coefficient	k_v	m s^{-1}	1.23E-09	2.45E-10
		m day^{-1}	1.06E-04	2.12E-05

Table 5. Parameters for analysis

Parameter	Symbol	Unit	Soft Clay	Hard Clay	Overburden
Unit Weight	γ	kN m^{-3}	16	20	20
Dry Unit Weight	γ_d	kN m^{-3}	14	18	16
Drained Shear Strength	S_d	kN m^{-2}	1	30	3
Effective Friction Angle	φ'	$\circ$	25	30	26
Poisson's Ratio	v		0.3	0.3	0.3
Initial Void Ratio	e_0		1.5	0.6	
Compression Index (λ=cc 2.303^{-1})	λ		0.259	0.086	
Swell Index (κ=cs 2.303^{-1})	κ	Day	0.026	0.008	
Horizontal Permeability Coefficient (k_h)	k_x, k_y	m day^{-1}	0.000265	0.000021	0.10
Vertical Permeability Coefficient (k_v)	k_z	m day^{-1}	0.000106	0.000021	0.01
Elastic Modulus	E	kN m^{-2}	1000	100000	10000

Note: No geotechnical investigation was carried out on overburden. Parameters were assumed.

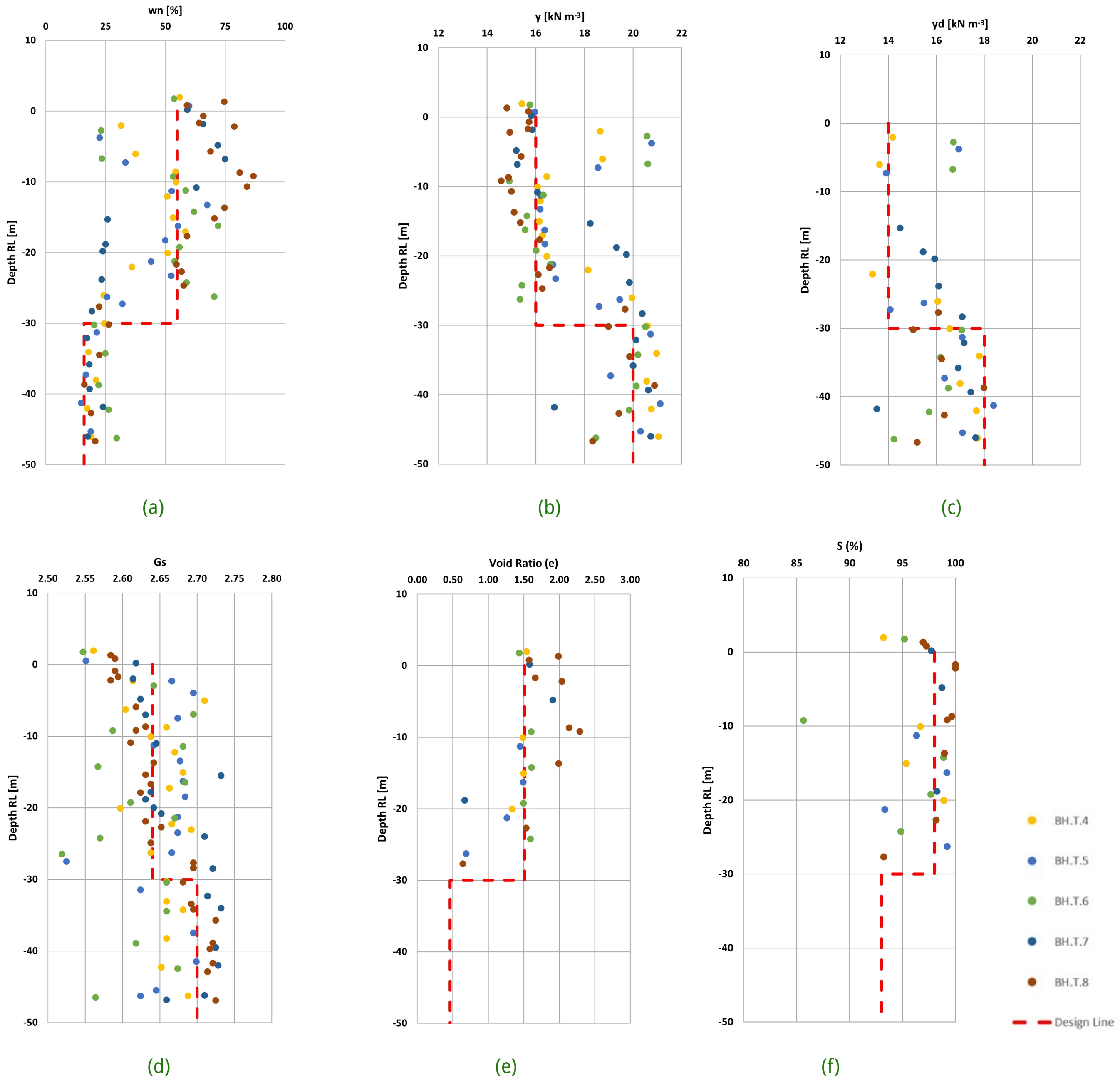

Figure 7 Index properties : water content vs depth (a), unit weight vs depth (b), dry unit weight vs depth (c), specific gravity vs depth (d), void ratio vs depth (e), degree of saturation vs depth (f)

Table 6. Analysis Case

Case	Condition	$k_x = k_y$ [m day^{-1}]	k_z [m day^{-1}]	k_h/k_v
1	Initial	0.000265	0.000106	2.5
2	Parameters	0.000530	0.000106	5.0
3		0.000795	0.000106	7.5
4		0.001060	0.000106	10.0
5		0.005300	0.000106	50.0
6		0.010600	0.000106	100.0
7	Amplification	0.02	0.004	5.0
8	Parameters	0.04	0.004	10.0
9		0.2	0.004	50.0
10		0.4	0.004	100.0

11. From Figure 8, the PI for the upper clay layer was 50, resulting in an effective friction angle of 25° after being plotted. For the lower layer, with PI = 24, the effective friction angle reached 30° after being plotted.

4 ANALYSIS RESULTS

4.1 Geometry Model

The analysis was performed using finite element software MIDAS GTS NX. The model was 2000 m long and 300 m wide. The soft clay soil was modeled using the soft soil model, while the overburden waste dump and hard clay were modeled using the Mohr-Coulomb

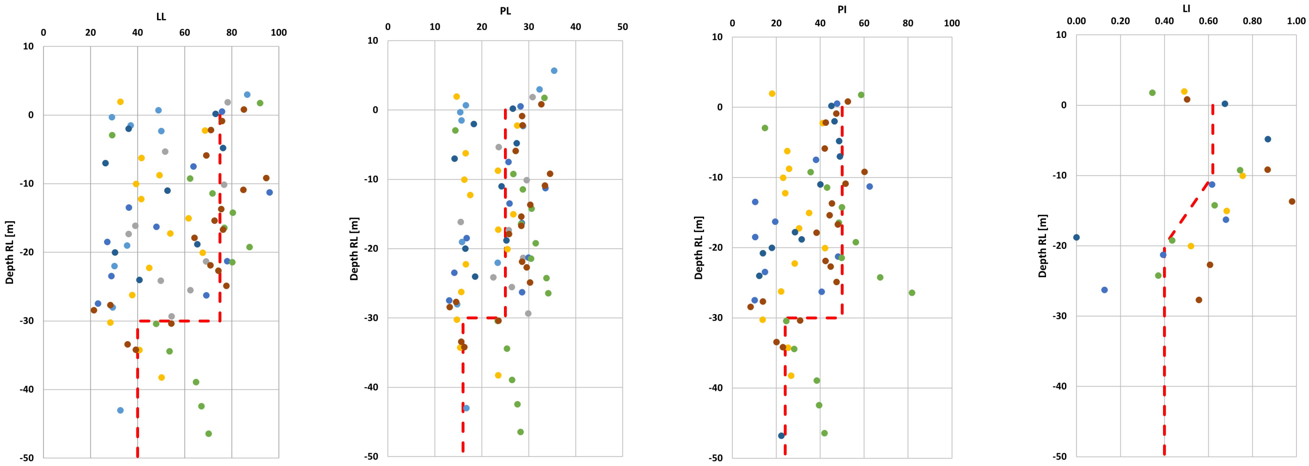

(a) (b) (c) (d)

Figure 8 Atterberg limits : liquid limit vs depth (a), plastic limit vs depth (b), plasticity index vs depth (c), liquidity index vs depth (d)

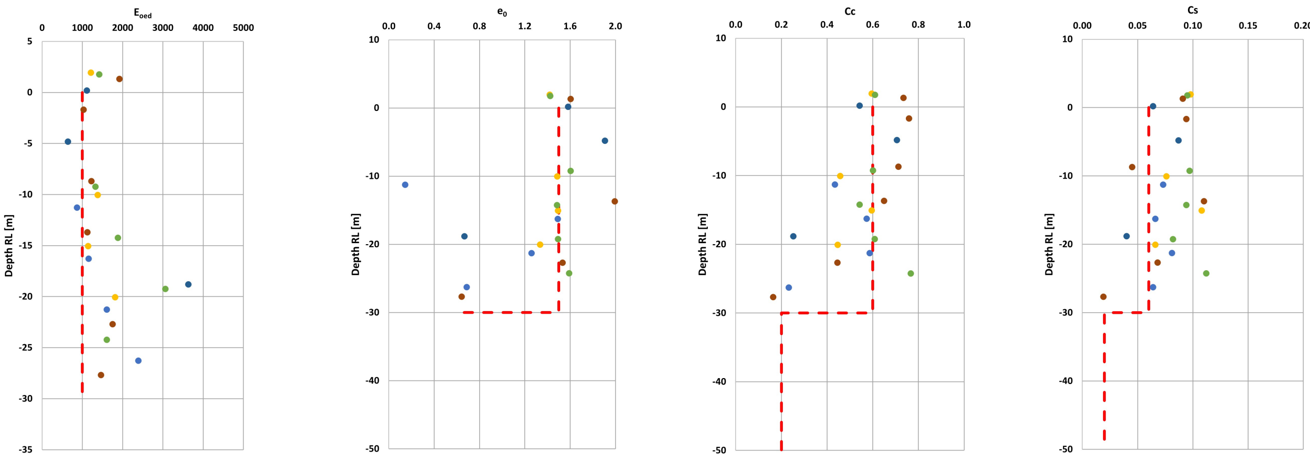

(a) (b) (c) (d)

Figure 9 Consolidation : E_{oed} vs depth (a), e_0 vs depth (b), compression index vs depth (c), swelling index vs depth (d)

model. The analysis primarily focuses on migrating excess pore pressure within the soft clay layer. Therefore, a more complex soil model was employed for the soft clay layer, while a simpler soil model was used for the two other layers. The soft soil model necessitates inputs for compression index (λ), swelling index (κ), OCR (overconsolidation ratio), and POP (preoverburden pressure) (Melnikov, 2016). The draining condition was set at the ground surface, where excess pore pressure equals zero. Drainage parameters utilized the undrained (effective stiffness/effective strength) option. The initial stress condition was not set using the k_0 condition option; instead, it employed the default condition, where stress is calculated based on depth. The position of the pipeline was modeled using the cutting diagram feature available in the software. As illustrated in Figure 12, the model comprises a single layer of soft clay (grey), two layers of hard clay (brown and blue), and three layers of overburden (purple, orange, and pink).

4.2 Stage Construction

A four-stage construction sequence was implemented using the consolidation stage type, encompassing the initial condition, and the construction of overburden layers 1, 2 and 3. The durations for the initial, overburden 1, 2, and 3 stages were 1, 1460, 120, and 60 days, respectively. Figure 13 illustrates the stage construction model, starting with the initial condition containing only soft clay and hard clay, followed by stage one incorporating the first overburden, stage two with the second overburden, and stage three with the final overburden.

4.3 Analysis

Analysis was carried out by varying the horizontal permeability coefficient while maintaining the value of the vertical permeability coefficient to observe the behavior of the excess pore pressure. The horizontal to vertical permeability coefficient (k_h/k_v) ratio was examined

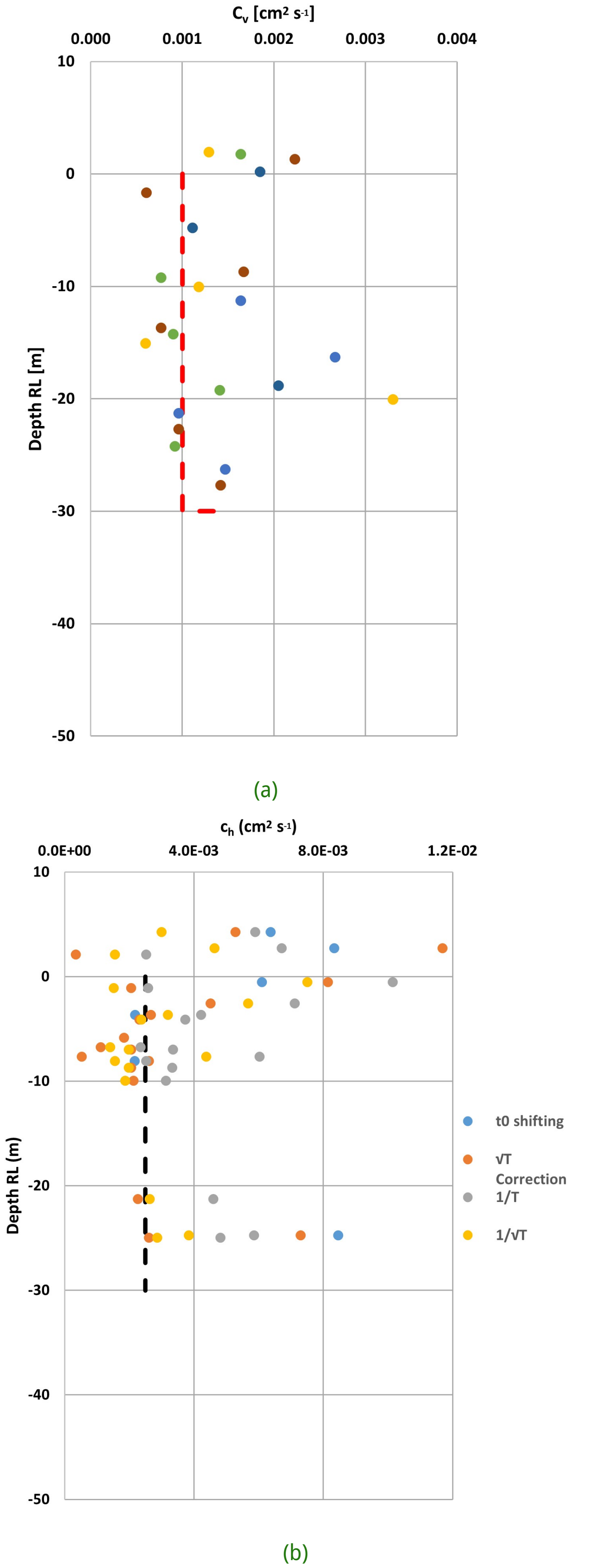

Figure 10 Vertical coefficient consolidation (a) and horizontal coefficient consolidation (b)

at intervals of 2.5, 5, 7.5, 10, 50 and 100 times. The horizontal and vertical permeability coefficients in the software were represented by the symbols k_x and k_y, respectively. The initial analysis was conducted using permeability coefficients estimated from the geotechnical investigation (initial permeability coefficient, case 1 to case 6 in Table 6). Subsequently, further analysis was carried out by amplifying the permeability coefficient values (case 7 to case 10 in Table 6).

4.3.1 Analysis Result using Initial Permeability Coefficient

Figure 13 illustrates the migration of excess pore pressure for conditions with k_h/k_v = of 2.5 and = 100. The excess pore pressure and displacement recorded at the pipeline location are presented in Figure 15. There is little difference in excess pore pressure between k_h/k_v = of 2.5 and = 100. Figure 15 shows the displacement difference across k_h/k_v ranging from 2.5 to 100, with only a slight reduction in excess pore pressure observed. In the model, however, the migration of excess pore pressure from left to right was observed. The recorded displacement increased by 4 mm with a ratio of 100 times.

4.3.2 Analysis Result using Amplified Permeability Coefficient

In Figure 16, the red color represents the maximum values of excess pore pressure. The analysis using the amplified permeability coefficient revealed a migration of larger excess pore pressure from the left to the right side of the model during the construction stage. As the k_h/k_v ratio increased, the magnitude of excess pore pressure migration also increased, as did the displacement. Figure 17 illustrates the comparison between different k_h values while keeping k_v constant, ranging from k_h = 0.02 and k_v = 0.004 (k_h/k_v =5) to k_h = 0.4 and k_v = 0.004 (k_h/k_v =100). An increase of approximately 44 kN m^{-2} in excess pore pressure and 42 cm in displacement were observed when comparing k_h/k_v ratios of 2.5 and 100.

4.4 Result Comparison

The initial and amplified analysis yielded similar results, demonstrating the migration of excess pore pressure from the left side to the right side of the model. The migration was only slightly visible when using initial condition parameters however, it becomes clearer when analyzed using amplified parameters (compare the left side of Figure 14 with the left side of Figure 16, or the right side of Figure 14 with the right side of Figure 16). The excess pore pressure and displacement measured at the pipeline location exhibited only slight differences when using initial parameters, but showed a significant increase when analyzed using amplified parameters.

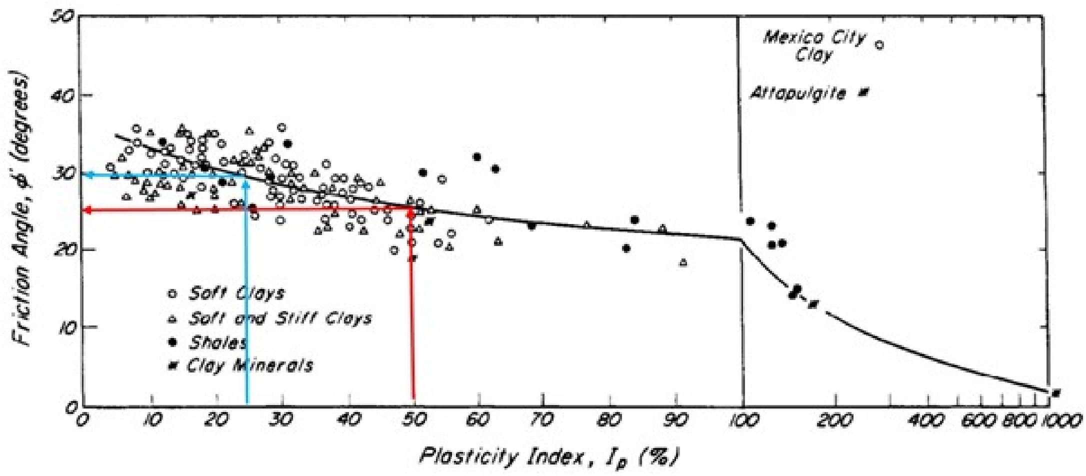

Figure 11 Effective friction angle (Terzaghi et al., 1996)

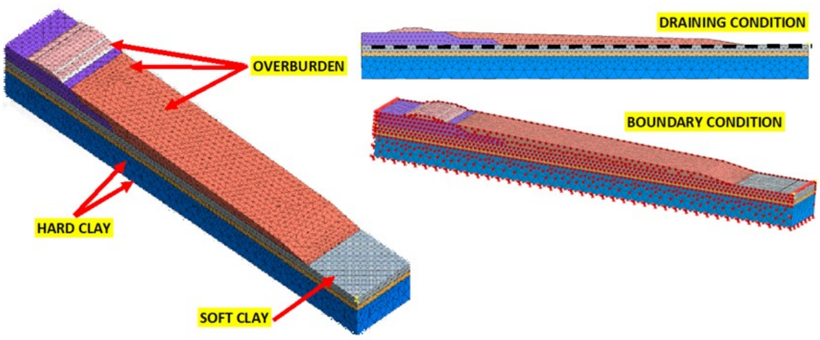

Figure 12 Geometry model in MIDAS GTS NX

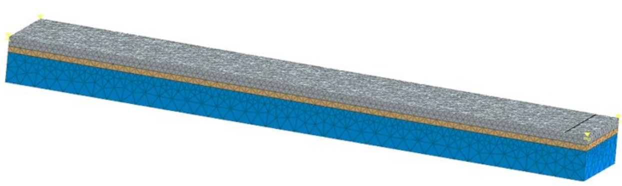

(a) Initial condition - no overburden

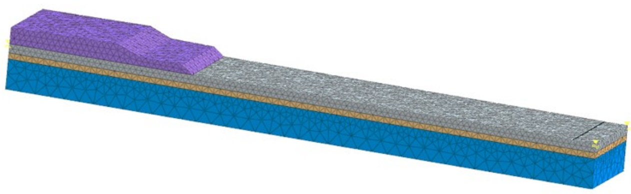

(b) Stage 1 - first overburden construction

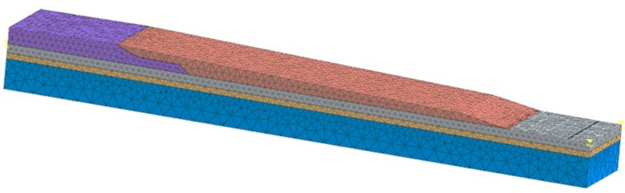

(c) Stage 2 - second overburden construction

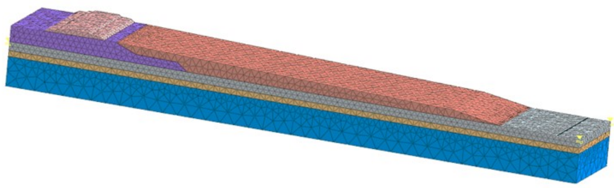

(d) Stage 3 - final overburden construction

Figure 13 Stage construction

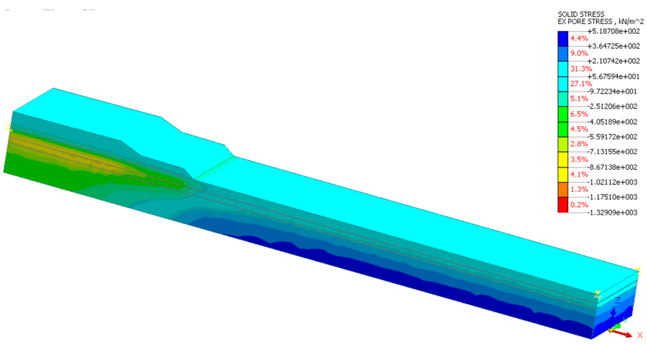

(a) Excess pore pressure during first overburden construction

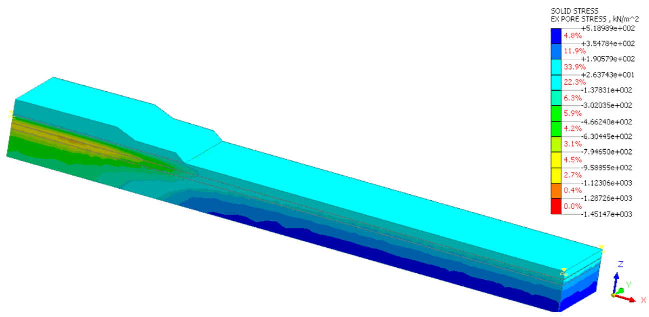

(b) Excess pore pressure during first overburden construction

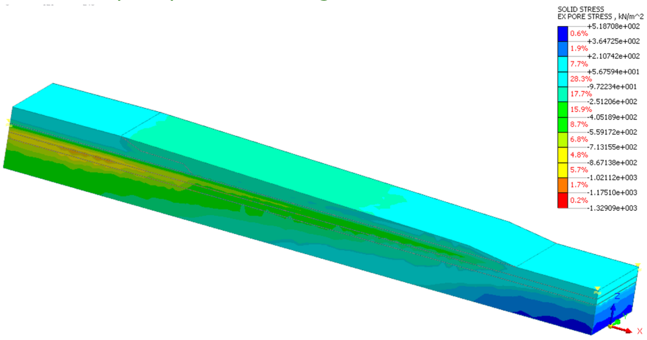

(c) Excess pore pressure during second overburden construction

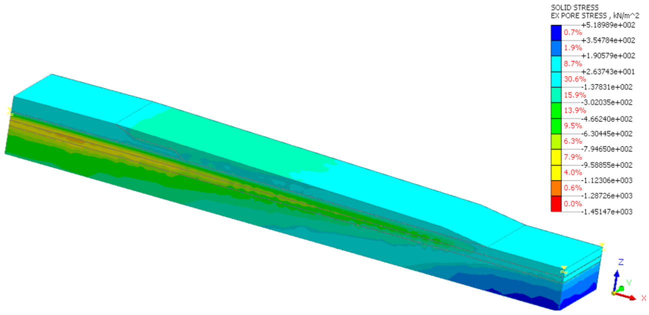

(d) Excess pore pressure during second overburden construction

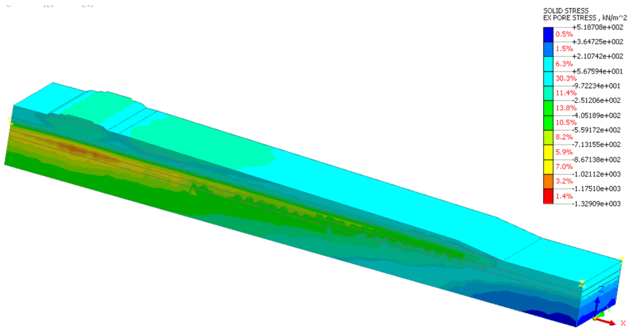

(e) Excess pore pressure during third overburden construction

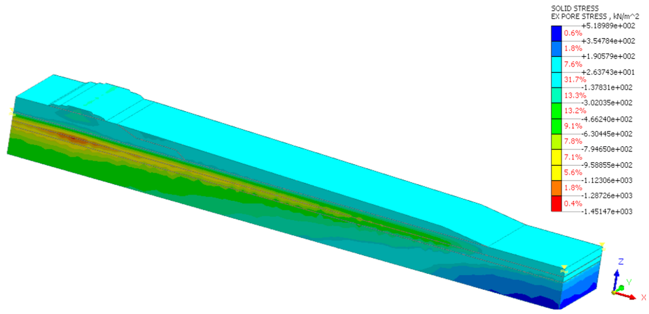

(f) Excess pore pressure during third overburden construction

Figure 14 Result from initial permeability coefficient k_h/k_v=2.5 (Left) and k_h/k_v=100 (Right)

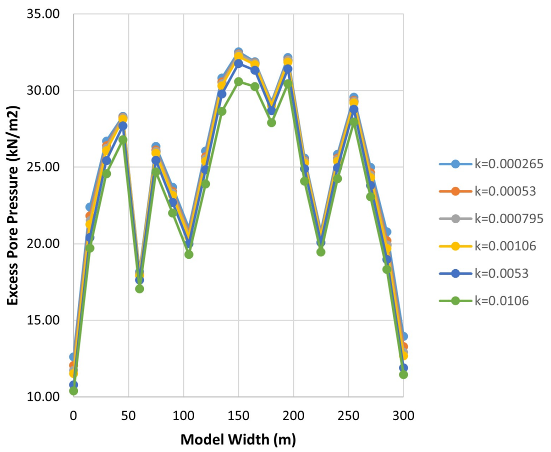

(a)

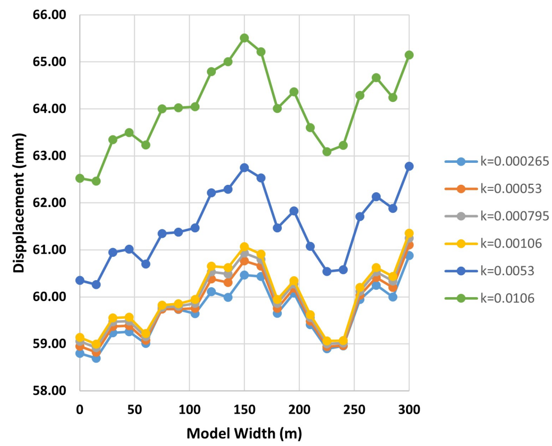

(b)

Figure 15 Excess pore pressure comparison (a) and displacement comparison (b) towards horizontal permeability coefficient

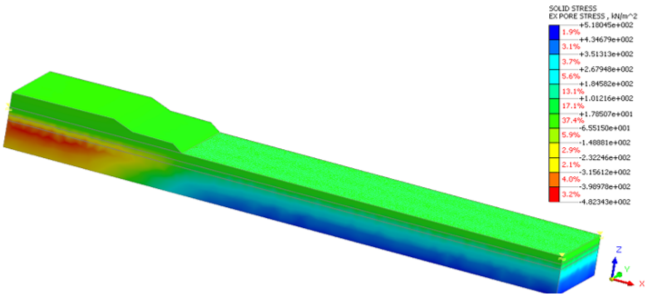

(a) Excess pore pressure during first overburden construction

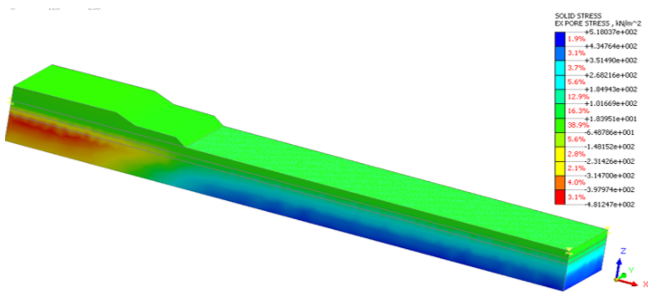

(b) Excess pore pressure during first overburden construction

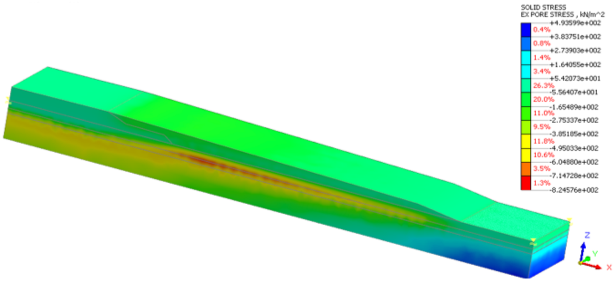

(c) Excess pore pressure during second overburden construction

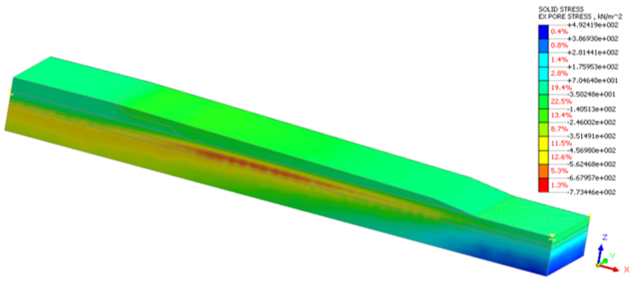

(d) Excess pore pressure during second overburden construction

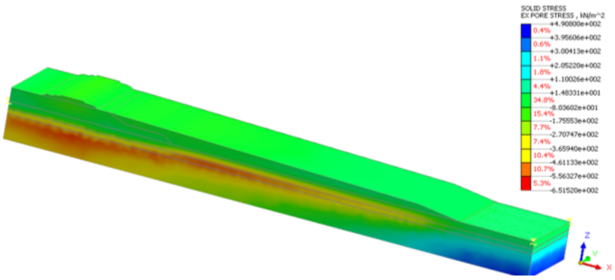

(e) Excess pore pressure during third overburden construction

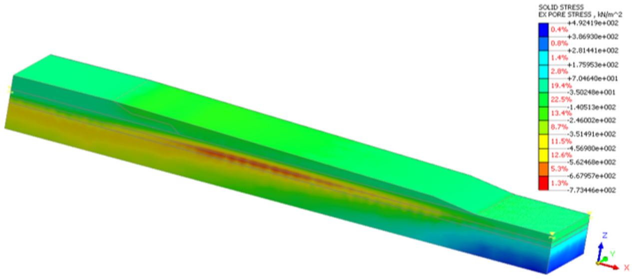

(f) Excess pore pressure during third overburden construction

Figure 16 Result from amplified permeability coefficient k_h/k_v=2.5 (left) and k_h/k_v=100 (right)

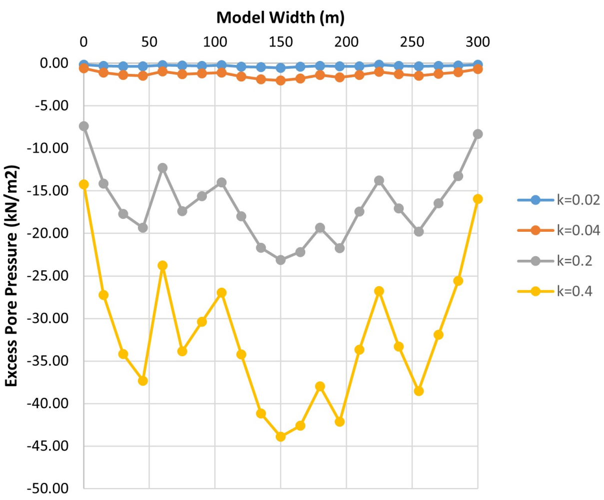

(a)

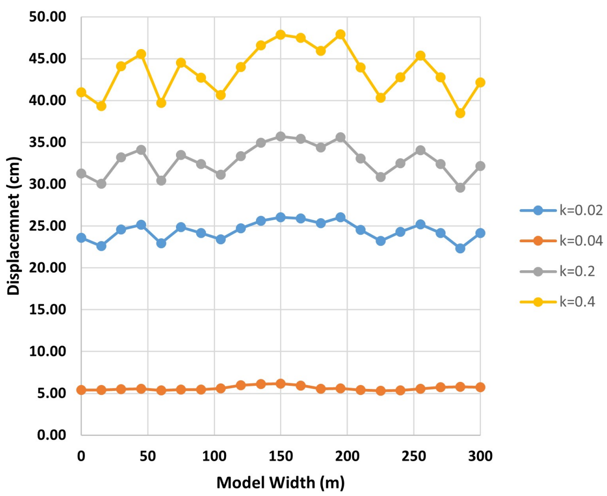

(b)

Figure 17 Excess pore pressure comparison (a) and displacement comparison (b) towards horizontal permeability coefficient

5 CONCLUSION

The permeability coefficient ratio of 1-1.5 times can generally lead to excess pore water pressure dissipation primarily in the vertical direction. This study demonstrated that the migration of excess pore water pressure can occur horizontally in alluvium soft clay when the ratio between horizontal and vertical permeability coefficient was significant. The initial analysis employing the in-situ permeability coefficient (k_h/k_v = 2.5), revealed that as k_h/k_v increases up to 100 times only a minor migration of excess pore water pressure occured, resulting in negligible displacement values. Further analysis using the amplified permeability coefficient (k_h = 0.02 m day^{-1} and k_v = 0.004 m day^{-1}) and increasing k_h/k_v ratio up to 100 times distinctly demonstrated the migration. The displacement reached up to 42 cm accompanied by a 44 kN m^{-2} increase in excess pore pressure measured at the pipeline location. The greater the ratio between the horizontal and vertical coefficients, the more extensive the migration of excess pore pressure leading to larger displacement.

The analysis results, however, do not accurately represent the actual condition where the pipeline was displaced horizontally by 6.8 m and thrusted upwards by 2.0 m. There may be other factors that were not considered or simplified in this study. Further and more comprehensive data should be collected to facilitate a more accurate analysis of the results. Nevertheless, the construction of a high embankment overlying a soft clay layer is recommended to consider the effect of the excess pore pressure migration on embankment stability.

DISCLAIMER

The authors declare no conflict of interest.

REFERENCES

Al-Khazaali, M. and Vanapalli, S. K. (2018), 'Axial force-displacement behaviour of a buried pipeline in saturated and unsaturated sand', *Géotechnique* pp. 1–66.
URL: *https://doi.org/10.1680/jgeot.17.p.116*

Balachowski, L. (2006), 'Soft soil overconsolidation and CPTu dissipation test', *Hydro-Engineering and Environmental Mechanics* **53**(2), 155–180.

Chai, J., Sheng, D., Carter, J. and Zhu, H. (2012), 'Coefficient of consolidation from non-standard piezocone dissipation curves', *Computers and Geotechnics* **41**, 13–22.
URL: *https://doi.org/10.1016/j.compgeo.2011.11.005*

Chung, S., Kweon, H. and Jang, W. (2014), 'Hyperbolic fit method for interpretation of piezocone dissipation tests', *Journal Geotechnical and Geoenvironmental Engineering* **140**(1), 251–254.
URL: *https://doi.org/10.1061/(ASCE)/GT.1943-5606.0000967*

Lim, B., Tumay, M., Lee, J., Jun, B. and Jung, J. (2014), 'A case study in evaluating the status of consolidation of a soft soil deposit by incomplete piezocone dissipation tests using laboratory and field data', *Soils and Foundations* **54**(4), 648–656.
URL: *https://doi.org/10.1016/j.sandf.2014.06.007*

Liu, S., Ju, J., Cai, G. and Liu, Z. (2014), 'Stress history estimation method of underconsolidated soil by partial piezocone dissipation tests', *Marine Georesources & Geotechnology* **32**, 368–378.
URL: *https://doi.org/10.1080/1064119X.2013.778376*

Melnikov, e. a. (2016), 'Ocr and pop parameters in plaxis-based numerical analysis of loaded over consolidated soils', *Procedia Engineering* **165**, 845–852.
URL: *https://doi.org/10.1016/j.proeng.2016.11.783*

Robertson, P. (2010), Estimating in-situ soil permeability from CPT & CPTu, *in* '2nd International Symposium on CPT'.

Shen, N., Qi, X., Shen, L., Li, B. and Yan, Y. (2009), Geological hazard assessment in the construction site of LNG pipeline project, *in* 'American Society of Civil Engineers International Conference on Pipelines and Trenchless Technology (ICPTT) 2009 - Shanghai, China', pp. 1532–1541.
URL: *https://doi.org/10.1061/41073(361)161*

Sully, J., Robertson, P., Campanella, R. and Woeller, D. (1999), 'An approach to evaluation of field CTPu dissipation data in overconsolidated fine-grained soils', *Journal of Canadian Geotech* **36**, 369–381.

Teh, C. and Houlsby, G. (1991), 'An analytical study of cone penetration test in clay', *Geotechnique* **41**(1), 17–34.
URL: *https://doi.org/10.1680/geot.1991.41.1.17*

Terzaghi, K., Peck, R. and Mesri, G. (1996), *Soil Mechanics in Engineering Practice*, 3rd edn, John Wiley & Sons, New York.

Trautmann, C. H. and O'Rourke, T. D. (1985), 'Lateral force-displacement response of buried pipe', *Journal of Geotechnical Engineering* **111**(9), 1077–1092.
URL: *https://doi.org/10.1061/(ASCE)0733-9410(1985)111:9(1077)*

Visnuvardhan, S., Murthy, A. and Choudhary, A. (2023), 'A review on pipeline failures, defects in pipelines and their assessment and fatigue life prediction methods', *International Journal of Pressure Vessels and Piping* **201**.
URL: *https://doi.org/10.1016/j.ijpvp.2022.104853*

Whittle, A., Sutabutr, T., Germaine, J. and Varney, A. (2001), 'Prediction and interpretation of pore pressure dissipation for a tapered piezoprobe', *Geotechnique* **51**(7), 601–617.
URL: *https://doi.org/10.1680/geot.2001.51.7.601*

Yuan, F., Li, L. and Guo, Z. (2014), Numerical study of landslide impact on submarine pipelines, *in* 'Proceedings of the ASME 2014 33rd International Conference on Ocean, Offshore and Arctic Engineering OMAE2014', San Francisco, USA.

Zhang, W. Y. and Askarinejad, A. (2021), 'Ultimate lateral pressures exerted on buried pipelines by the initiation of submarine landslides', *Landslides* **18**, 3337–3351.
URL: *https://doi.org/10.1007/s10346-021-01711-8*

Zhang, Y. et al. (2022), 'Pore pressure response and dissipation of piezocone test in shallow silty soil of yellow river delta', *Journal of Marine Science and Engineering* **10**(2), 255.
URL: *https://doi.org/10.3390/jmse10020255*

[This page is intentionally left blank]